AD-A163 219 RESONANCE FLUORESCENCE OF A TWO-LEVEL ATOM NEAR A ROUGH METAL SURFACE (U) STATE UNIV OF NEW YORK AT BUFFALO DEPT OF CHEMISTRY X HUANG ET AL JAN 86 1/1

UNCLASSIFIED UROCHESTER/DC/85/TR-4 N00014-86-K-0043 F/G 7/5 NL

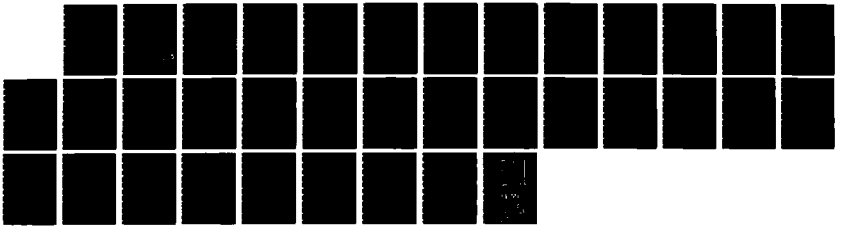

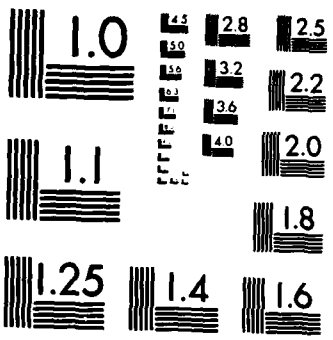

(12)

OFFICE OF NAVAL RESEARCH

Contract N00014-86-K-0043

TECHNICAL REPORT No. 4

Resonance Fluorescence of a Two-Level Atom Near a Rough Metal Surface

by

Xi-Yi Huang, Ki-Tung Lee and Thomas F. George

Prepared for Publication

in

Journal of Chemical Physics

Departments of Chemistry and Physics
State University of New York at Buffalo
Buffalo, New York 14260

January 1986

UNCLASSIFIED

SECURITY CLASSIFICATION OF THIS PAGE

REPORT DOCUMENTATION PAGE

1a. REPORT SECURITY CLASSIFICATION Unclassified	1b. RESTRICTIVE MARKINGS
2a. SECURITY CLASSIFICATION AUTHORITY	3. DISTRIBUTION/AVAILABILITY OF REPORT Approved for public release; distribution unlimited
2b. DECLASSIFICATION/DOWNGRADING SCHEDULE	
4. PERFORMING ORGANIZATION REPORT NUMBER(S) UBUFFALO/DC/85/TR-4	5. MONITORING ORGANIZATION REPORT NUMBER(S)
6a. NAME OF PERFORMING ORGANIZATION Depts. Chemistry & Physics State University of New York 6b. OFFICE SYMBOL (If applicable)	7a. NAME OF MONITORING ORGANIZATION
6c. ADDRESS (City, State and ZIP Code) Fronczak Hall, Amherst Campus Buffalo, New York 14260	7b. ADDRESS (City, State and ZIP Code) Chemistry Program 800 N. Quincy Street Arlington, Virginia 22217
8a. NAME OF FUNDING/SPONSORING ORGANIZATION Office of Naval Research 8b. OFFICE SYMBOL (If applicable)	9. PROCUREMENT INSTRUMENT IDENTIFICATION NUMBER Contract N00014-86-K-0043
8c. ADDRESS (City, State and ZIP Code) Chemistry Program 800 N. Quincy Street Arlington, Virginia 22217	10. SOURCE OF FUNDING NOS. PROGRAM ELEMENT NO. / PROJECT NO. / TASK NO. / WORK UNIT NO.

11. TITLE
Resonance Fluorescence of a Two-Level Atom Near a Rough Metal Surface

12. PERSONAL AUTHOR(S)
Xi-Yi Huang, Ki-Tung Lee and Thomas F. George

13a. TYPE OF REPORT	13b. TIME COVERED	14. DATE OF REPORT (Yr., Mo., Day)	15. PAGE COUNT
Interim Technical	FROM _____ TO _____	January 1986	24

16. SUPPLEMENTARY NOTATION
Prepared for publication in the Journal of Chemical Physics

17. COSATI CODES			18. SUBJECT TERMS (Continue on reverse if necessary and identify by block number)
FIELD	GROUP	SUB. GR.	RESONANCE FLUORESCENCE, SURFACE DRESSED, TWO-LEVEL ATOM, ROUGH METAL SURFACE, LASER DRIVEN, ADATOM-HEMISPHEROID

19. ABSTRACT (Continue on reverse if necessary and identify by block number)

Surface-dressed optical Bloch equations are solved for a two-level atom near or adsorbed on a rough surface, which is modeled as a hemispheroid protrusion on a perfectly-conducting surface. Effects of the laser bandwidth are included by means of a phase-diffusion model. The presence of the surface roughness generates a dephasing broadening mechanism on the adatomic resonance fluorescence spectrum, which can be strongly enhanced by plasmon resonances depending on the shape of the hemispheroid. The dependence of the electrodynamics of the adatom on the adatom-hemispheroid distance is also evaluated.

20. DISTRIBUTION/AVAILABILITY OF ABSTRACT	21. ABSTRACT SECURITY CLASSIFICATION
UNCLASSIFIED/UNLIMITED ☒ SAME AS RPT. ☒ DTIC USERS ☐	Unclassified

22a. NAME OF RESPONSIBLE INDIVIDUAL	22b. TELEPHONE NUMBER (Include Area Code)	22c. OFFICE SYMBOL
Dr. David L. Nelson	(202)696-4410	

DD FORM 1473, 83 APR ...ON OF 1 JAN 73 IS OBSOLETE.

UNCLASSIFIED

SECURITY CLASSIFICATION OF THIS PAGE

Journal of Chemical Physics, in press

Resonance Fluorescence of a Two-Level Atom Near a Rough Metal Surface

Xi-Yi Huang
Department of Chemistry
University of Rochester
Rochester, New York 14620

Ki-Tung Lee
Department of Chemistry
Illinois Institute of Technology
Chicago, Illinois 60616

Thomas F. George
Departments of Chemistry and Physics
State University of New York at Buffalo
Buffalo, New York 14260

Abstract

Surface-dressed optical Bloch equations are solved for a two-level atom near or adsorbed on a rough surface, which is modeled as a hemispheroid protrusion on a perfectly-conducting surface. Effects of the laser bandwidth are included by means of a phase-diffusion model. The presence of the surface roughness generates a dephasing broadening mechanism on the adatomic resonance fluorescence spectrum, which can be strongly enhanced by plasmon resonances depending on the shape of the hemispheroid. The dependence of the electrodynamics of the adatom on the adatom-hemispheroid distance is also evaluated.

1. Introduction

There is considerable interest in the interaction of laser radiation with adspecies on surfaces.[1] In particular, researchers have studied the problem of surface-enhanced spontaneous emission of two-level atoms near a mirror[2-5] and decay of excited molecules near a small metal sphere.[6] The enhancement of Raman scattering and fluorescence by small metal spheres has also been examined.[7,8] However, when the resonant, driving coherent radiation is very strong, interesting "resonance fluorescence" and other nonlinear phenomena can occur.[9,10] In these cases, the resonant laser puts the atom or molecule in an environment where the probability of stimulated emission can exceed that of spontaneous emission. Under these circumstances we find back-transitions and Rabi oscillations of state probability amplitudes, and the dynamic Stark splitting of resonances and mutational oscillations of the emitted light intensity become important parts of the laser-driving process.[9,10] In a strong resonant field, nonlinear scattering occurs, and multiphoton processes become as important as single-photon processes, so that we can no longer rely on the conventional low-order perturbation theory of fluorescence. In the surface-free case, i.e., in the absence of a solid surface or when the atom is very far from the surface, resonance excitation of a two-level atom by a laser field has been extensively investigated, using the powerful optical Bloch equations.[9,10] Previously, we have derived a set of surface-dressed optical Bloch equations[11-15] by which we can discuss the effects of the surface-reflected photons, the resonance interaction between the adatom and surface-plasmons, the collision dephasing of the adatom produced by gas atoms in the medium, and the random phase fluctuation of the (intense) laser field. In the present paper, we extend the calculation of the resonance fluorescence for a flat-surface[7-8] to the case of an interface with metallic protrusions.

Surface roughness can be characterized as a set of protrusions which randomly (or regularly, in the case of a grating) stick out of the underlying planar substrate. While the protrusions may have different sizes and shapes, in this paper we model the protrusions as a prolate hemispheroid on top of a plane,[16,17] as depicted in Fig. 1. We note that the model of a half spheroid on a flat perfect conductor[16] has been shown to be identical to a full spheroid in a vacuum.[1b] Thus the following discussion can be also used for ellipsoidal cases. The two-level adatom, which is located at a distance d from the top of the hemispheroid, is driven by a laser. The adatom has no dipole moment in its ground state, but it can have a transition dipole connecting the ground and excited states. The emitted photons will be reflected by the flat mirror and the hemispheroid, which in turn provide a resonance feedback to the dynamics of the adatom. The spectrum of laser light scattering in the presence of a bump-plane surface system near a two-level atom is then the subject of this paper.

2. Surface-Dressed Optical Bloch Equations for a Rough Surface

Let us evaluate the light scattering produced when a laser field is incident on a molecule adsorbed on a rough surface. The surface will be taken to be a prolate hemispheroid protruding from a flat plane. The spheroid is assumed to have the complex dielectric constant $\varepsilon(\omega)$, while the plane is taken to be a perfect conductor. The incident laser field is taken to be propagating along the interface, where its electric field is taken to be along the normal of the interface. The prolated spheroidal coordinate (ξ, η, ϕ) system[18] is used to calculate the reflected field. We define

$$\xi_1 = (a + d)/f$$

$$\xi_0 = a/f$$

and

$$f = (a^2 - b^2)^{1/2} \quad ,$$

where a and b are the semi-major and semi-minor axes of the hemispheroid (Fig. 1). The reflected field at the position of the adatom (dipole), in the limit of the near-field approximation, can be written as[16]

$$E_r = -\frac{1}{f} \sum_n{}' C_n \, Q_n'(\xi_1) + \frac{\mu}{4(f\xi_1)^3} \tag{1}$$

where Q_n denotes the Legendre function of the second kind and μ is the induced dipole moment which will be given later. The expansion coefficient C_n is given by

$$C_n = \frac{(\varepsilon - 1)E_0 + \xi_0 \, \delta_{n,1}}{\varepsilon Q_1(\xi_0) - \xi_1 Q_1'(\xi_0)} + \frac{4n + 2}{f^2} \mu \frac{(1 - \varepsilon)P_n'(\xi_0)Q_n'(\xi_1)P_n(\xi_0)}{\varepsilon Q_n(\xi_0)P_n'(\xi_0) - Q_n'(\xi_0)P_n(\xi_0)} \quad , \tag{2}$$

where P_n denotes the Legendre function of the first kind and E_0 is the amplitude of the incident laser. The induced dipole moment, μ, of the adatom is given by

$$\mu = \alpha E_{total} \quad ,$$

where α is the polarizability along the semi-major axis and E_{total} is the total

electric field applied to the adatom. The induced dipole moment can be expressed by

$$\mu = \alpha(-\frac{1}{f}\sum_{n}{}' C_n Q_n'(\xi_1) + \frac{\mu}{4(f\xi_1)^3} + E_0) \quad . \tag{3}$$

After rearranging Eq.(3) and substituting back to Eq.(1), we obtain

$$E_r = \frac{E_0}{1-\Gamma}\left[\frac{(1-\varepsilon)\xi_0 Q_1'(\xi_1)}{\varepsilon Q_1(\xi_0) - \xi_0 Q_1'(\xi_0)} + \Gamma\right] \quad , \tag{4}$$

where

$$\Gamma = \frac{\alpha}{4(f\xi_1)^3} + \frac{2\alpha}{f^3}(\varepsilon - 1)\sum_{n}{}' \frac{(2n+1)P_n'(\xi_0)[Q_n(\xi_1)]^2 P_n(\xi_0)}{\varepsilon Q_n(\xi_0)\, P_n'(\xi_0) - Q_n'(\xi_0)\, P_n(\xi_0)} \quad .$$

As shown in Eq.(4), there are two resonance conditions: $1-\Gamma$ approaches zero and ε equals $\xi_0 Q_1'(\xi_1)/Q_1(\xi_0)$. It can be shown easily that the near-field approximation will break down when the factor $1-\Gamma$ approaches zero. The physical interpretation of this factor is the image enhancement effect. The importance of the image effect has been reviewed by Schatz.[19] Let us focus on the second resonance condition. We recall that

$$Q_1(\xi) = \frac{\xi}{2}\ln\left[\frac{\xi+1}{\xi-1}\right] - 1 \quad .$$

Hence, we can write the second resonance condition as

$$\varepsilon = \frac{(\xi_0/2)\ln[(\xi_0+1)/(\xi_0-1)] - \xi_0^2/(\xi_0^2-1)}{(\xi_0/2)\ln[(\xi_0+1)/(\xi_0-1)] - 1} \quad . \tag{5}$$

Using the identity

$$(\xi^2 - 1)^{-1} = \sum_{n} \xi^{-2n}$$

we obtain

$$\varepsilon = 1 - \frac{1}{Q_1(\xi_0)(\xi_0^2 - 1)} \quad . \tag{6}$$

In the limit $\xi_0 \to \infty$ such that the spheroid tends towards a sphere, Eq.(6)

becomes

$$\varepsilon(\xi_0 \to \omega) = 1 - \frac{3\xi_0^2}{\xi_0^2 - 1} \approx -2 \quad , \tag{7}$$

which reduces to the usual surface plasmon resonance condition of a sphere, $\varepsilon + 2 = 0$. We will discuss below how to use this reflected field to calculate the transition dipole.

To treat problems of excitation and dissipation of a two-level adatom near a hemispheroid, a self-consistent approach is developed in which the dynamical behavior associated with the induced transition dipole is determined by surface dressed optical Bloch equations (SBE).[11,12] Essentially, the SBE are quantum operator equations for $\hat{\sigma}_{12}$, $\hat{\sigma}_{21}$ and $\hat{W}$, where $\hat{\sigma}_{ij} = |i\rangle\langle j|$ $(i,j = 1,2)$ are the adatomic transition operators and $\hat{W}(t) = \hat{\sigma}_{22}(t) - \hat{\sigma}_{11}(t)$ is the population inversion of the adatom. By defining

$$\hat{S}_{12}(t) = \hat{\sigma}_{12}(t) \exp(i\omega_L t) \tag{8}$$

$$\hat{S}_{21}(t) = \hat{\sigma}_{21}(t) \exp(-i\omega_L t) \tag{9}$$

where ω_L is the laser frequency, we can write the rotating-wave approximation (RWA) for the SBE of the adatom-bump system as

$$\frac{d}{dt}\begin{bmatrix} \hat{S}_{21}(t) \\ \hat{W}(t) \\ \hat{S}_{12}(t) \end{bmatrix} = \begin{bmatrix} -\tilde{\gamma}_2 + i\Delta & \frac{i\Omega^-(t)}{2} & 0 \\ i\Omega^+(t) & -\gamma_1 & -i\Omega^-(t) \\ 0 & \frac{-\Omega^+(t)}{2} & -\tilde{\gamma}_2 - i\Delta \end{bmatrix} \begin{bmatrix} \hat{S}_{21}(t) \\ \hat{W}(t) \\ \hat{S}_{12}(t) \end{bmatrix} - \gamma_1 \begin{bmatrix} 0 \\ 1 \\ 0 \end{bmatrix} .$$

$\Omega^{\pm}(t) = \Omega \exp[\mp i\phi(t)]$ is the time-dependent Rabi frequency, where $\Omega = (2/\hbar)\,|\mu_{21}|\,E_0(t)$ and $E(t)$ is written as an expectation value in a coherent state of the laser field in terms of the phase factor $\varphi(t)$ as $E(t) = E_0(t) \exp[-i\omega_L t + i\phi(t)] + c.c.$; $\Delta = \omega_{21} - \omega_L$ is the detuning; the surface-induced phase-decay $\tilde{\gamma}_2 = \gamma_2 + \gamma_s$, where γ_s is determined by the

reflected field which is emitted by the induced adatom and reflected by the bump-plane interface. In the case of a rough surface, γ_s is given by[11,12]

$$\gamma_s = (2/\hbar)\,\mathrm{Im}(F) \quad , \tag{11}$$

where

$$F = \frac{1}{1 - \Gamma}\left[\frac{(1 - \varepsilon)\,\xi_0 Q_1'(\xi_1)}{\varepsilon\, Q_1(\xi_0) - \xi_1 Q_1'(\xi_0)} + \Gamma\right] \quad .$$

To include the effects of the laser bandwidth γ_L, the phase-diffusion model for the laser field has been used by defining the following correlation function for the Rabi frequency:

$$\langle\langle\, \Omega^-(t_1)\, \Omega^+(t_2) \,\rangle\rangle = \Omega^2 \exp(-\gamma_L\, |t_2 - t_1|) \quad , \tag{12}$$

where the double bracket signifies two averages: one is over the stochastic ensemble and the other is a quantum mechanical average.

In the weak-field or large-detuning cases, where $W(t) = \langle\langle\, \hat{W}(t) \,\rangle\rangle = -1$, the population inversion of the two-level adatom has the following analytical form (for $t \geq 0$):

$$W(t) = -1 + \Omega^2 \left\{\frac{\tilde{\gamma}_2 + \gamma_L}{\gamma_1[(\tilde{\gamma}_2 + \gamma_L)^2 + \Delta^2]} + \frac{\gamma_1 - \tilde{\gamma}_2 - \gamma_L}{\gamma_1[(\gamma_1 - \tilde{\gamma}_2 - \gamma_L)^2 + \Delta^2]} \exp(-\gamma_1 t)\right.$$

$$- \frac{[(\tilde{\gamma}_2 + \gamma_L)(\gamma_1 - \tilde{\gamma}_2 - \gamma_L) + \Delta^2]\cos(\Delta t) + \Delta(2\tilde{\gamma}_2 - 2\gamma_L - \gamma_1)\sin(\Delta t)}{[(\tilde{\gamma}_2 + \gamma_L)^2 + \Delta^2][(\gamma_1 - \tilde{\gamma}_L - \gamma_L)^2 + \Delta^2]}$$

$$\left. \times \exp[-(\tilde{\gamma}_2 + \gamma_L)t] \right\} \quad . \tag{13}$$

The corresponding power spectrum $S(\omega)$ for the scattered light of the laser can be calculated through the Fourier transform of the dipole-dipole correlation function $\langle\langle \hat{S}_{21}(t_2)\hat{S}_{12}(t_1)\rangle\rangle$:

$$S(\omega) = \frac{\Omega^2}{2} \frac{1}{(\tilde{\gamma}_2 + \gamma_L)^2 + \Delta^2} \{ \frac{1}{(\tilde{\gamma}_2 - \gamma_L)^2 + \Delta^2}$$

$$\times [\frac{\gamma_L(\tilde{\gamma}_2^2 - \gamma_L^2 + \Delta^2) + 2\gamma_L \Delta(\omega - \omega_L)}{\gamma_L^2 + (\omega - \omega_L)^2} - \frac{\tilde{\gamma}_2(\tilde{\gamma}_2^2 - \gamma_L^2 + \Delta^2) + 2\gamma_L \Delta(\omega - \omega_{21})}{\tilde{\gamma}_2^2 + (\omega - \omega_{21})^2}]$$

$$+ \frac{2(\tilde{\gamma}_2 + \gamma_L)\tilde{\gamma}_2}{\gamma_1[\tilde{\gamma}_2^2 + (\omega - \omega_{21})^2]} \} . \qquad (14)$$

The spectrum of light scattering in Eq.(14) exhibits two spectral peaks which are strongly influenced by the resonance interaction between the adatom and the bump-flat surface system in Eq.(6). One peak is centered at $\omega = \omega_L$, which corresponds to elastic or Rayleigh scattering, and the other peak is near $\omega = \omega_{21}$, corresponding to inelastic scattering or fluorescence.

In another limit, i.e., the case of a very strong driving field, nonlinear scattering and multiphoton excitation processes can be as important as single-photon processes. The scattering light spectrum $S(\omega)$ of the adatom at steady state can obtain by solving tne SBE [Eq.(10)] to obtain the dipole-dipole correlation function. The result is

$$S(\omega) = \frac{\Omega^2}{\Delta^2 + \alpha\Omega^2} \{ \frac{\Delta^2 + \tilde{\gamma}_2}{\Delta^2 + \alpha\Omega^2} \delta(\omega - \Omega_L)$$

$$+ \frac{\Omega^2[(2\alpha - 1)\Delta^2 + \alpha^2\Omega^2]}{(\Delta^2 + \Omega^2)(\Delta^2 + \alpha\Omega^2)} [\frac{S_0/\pi}{(\omega - \omega_L)^2 + S_0^2}]$$

$$+ \frac{1}{2} \frac{(\Omega' - \Delta)[\alpha(\Omega' - \Delta) + \Delta]}{(\Delta^2 + \Omega^2)} [\frac{S_\pm/\pi}{(\omega - \omega_L + \Omega')^2 + S_\pm^2}]$$

$$+ \frac{1}{2} \frac{(\Omega' + \Delta)[\alpha(\Omega' + \Delta) - \Delta]}{(\Delta^2 + \Omega^2)} [\frac{S_\pm/\pi}{(\omega - \omega_L - \Omega')^2 + S_\pm^2}] \} , \qquad (15)$$

where the parameter α is defined as

$$\alpha = \tilde{\gamma}_2/2\gamma_2 \quad . \tag{16}$$

In Eq.(15), we have assumed zero laser bandwidth, $\gamma_L = 0$. The detuning parameter is defined as

$$\Omega' = \Delta + \Delta_s \tag{17}$$

where

$$\Delta_s = \Delta\{[1 + (\Omega/\Delta)^2]^{1/2} - 1\} \quad , \tag{18}$$

and the widths of the profiles are

$$S_0 = 2\gamma_2 \left(\frac{2\Omega^2 + \Delta^2}{\Omega^2 + \Delta^2}\right) \tag{19}$$

$$S_{\pm} = S_+ = S_- = \gamma_2\left[\frac{(1 + \alpha)\Omega + 2\alpha\Delta^2}{\Omega^2 + \Delta^2}\right] \quad . \tag{20}$$

Eq.(15) was derived under the assumption of a very strong coherent laser field, i.e., $\Omega^2 + \Delta^2 >> \tilde{\gamma}_2^2$. The strong-field spectrum, Eq.(15), has three spectral peaks: the coherent and incoherent parts of the Rayleigh scattering centered at $\omega = \omega_L$ and the two side bands centered at $\omega = \omega_L \pm \Omega'$ due to a multiphoton process and fluorescece of the adatom, referred to as the three-photon fluorescence components, respectively.[11] We shall see in the next section how the resonance coupling between adatom and bump influences the strong-field three-peak spectrum.

3. Numerical Results

Using Eqs.(13), (14) and (15), which describe the excitation and relaxation behavior of a two-level atom near or adsorbed on a metal surface with roughness (a bump on a flat surface), we have evaluated numerically some typical cases for the rough surface-modified resonance fluorescence spectrum. In all the calculations, the laser photon energy is taken to be 2.75 eV.

Figure 2 displays the rough surface-induced phase-decay constant γ_s as a function of the semi-minor axis b of the surface protrusion, with the semi-major axis a for the surface protrusion fixed at 100 A. There is a sharp resonance peak at b ≈ 38 A, corresponding to a resonant excitation of plasmons in the bump which can strongly enhance adatom-bump interaction, through the reflected field at the atomic site. Figures 3(a) and (b) display the influence of the plasmon resonance in the bump on the adatomic population distribution. The time oscillations of the population will decrease as the semi-minor axis b of the spheroidal bump approaches the plasmon resonance b ≈ 38 A [Fig. 3(b)], indicating that the enhancement of the adatom-bump coupling leads to more damping of the adatomic oscillator.

Figure 4 displays the resonance fluorescence spectrum in the weak-field driving case [Eq.(14)], consisting of the Rayleigh and fluorescence peaks. The former peak in our model is determined by the laser bandwidth γ_L. The latter peak (fluorescence) strongly depends on the adatom-bump distance and the resonance coupling between the adatom and the bump. When the detuning Δ gets smaller and the semi-minor axis b of the bump spheroid reaches the plasmon resonance condition [see Fig. 4(b)], the two peaks will overlap, where the fluorescence peak is strongly broadened by resonant adatom-bump coupling. In this case, the height of the Rayleigh peak will depend on the atom-bump distance and parameter b.

Figure 5 displays the typical three-peak spectrum of the strong-field-driven adatom using the formula of Eq.(15). In Fig. 5(a) we can distinguish the Rayleigh (central) peak, the three-photon peak (left) and the fluorescence peak (right). In these pictures we have drawn just the profile of the incoherent component of the Rayleigh scattering, as the coherent component will not be broadened by the surface bump.

In the smaller detuning case, i.e., Fig. 5(a), the spectrum has a distinctive three-peak nature. In this case, the three-photon peak (left) has measurable height, which is almost comparable with the fluorescence peak. It is seen that the smaller the adatom-bump distance, the larger the broadening equally in the three spectral peaks, due to the enhancement of the adatom-bump coupling for smaller distances. In the larger detuning case, i.e., Fig. 5(b), the driving effect of the applied laser field is weaker due to the large detuning Δ. The height of the three-photon peak is decreased and the three-peak spectrum is transformed to the weak-field two-peak structure. In this case, smaller adatom-surface distances still lead to larger broadening, as in the former case.

4. Summary

A simple model has been developed to describe the influence of surface roughness on the dynamic behavior of a two-level adatom near a metal surface. Surface-dressed optical Bloch equations (SBE), which account for surface-reflected photons and the resonance interaction due to plasmon excitation in the metal protrusion, have been derived. Based on the SBE, the population distribution of the adatom and the power spectrum of the scattered light, as well as the surface-enhanced dephasing broadening of the atomic spectrum, have been evaluated. Collisions with foreign gas atoms and effects of the laser bandwidth can also be considered in our model. It is shown that the spectrum of scattered light, as well as the level population of the adatom, are strongly enhanced by the resonantly excitation of plasmons in the hemispheroid on the metal surface. The displayed surface enhancement for the adatom-bump system should be very useful in understanding the spectroscopy and chemistry associated with rough surface.

Acknowledgments

This research was supported by the Office of Naval Research and the Air Force Office of Scientific Research (AFSC), United States Air Force, under Contract F49620-86-C-009. The United States Government is authorized to reproduce and distribute reprints for governmental purposes notwithstanding any copyright notation hereon. We acknowledge stimulating discussion with Professor David Ronis.

References

1. (a) For a comprehensive review, see Surface-Enhanced Raman Scattering, ed. by R. K. Chang and T. E. Furtak (Plenum, New York, 1982); (b) H. Metiu, Prog. Surf. Sci. 17, 153 (1984); (c) H. Metiu and P. Das, Ann. Rev. Phys. Chem. 35, 507 (1984); (d) M. Moscovitz, Rev. Mol. Phys. 57, 783 (1985).
2. V. L. Lyaboshitz, Sov. Phys. JETP 26, 937 (1968).
3. H. Morawitz, Phys. Rev. 187, 1972 (1969).
4. P. W. Milonni and P. L. Knight, Opt. Commun. 9, 119 (1973).
5. G. S. Agarwal, Opt. Commun. 42, 205 (1982).
6. R. Ruppin, J. Chem. Phys. 76, 1681 (1982).
7. P. Das and H. Metiu, J. Phys. Chem. 89, 4681 (1985).
8. D. A. Weitz, S. Garoff, J. I. Gersten and A. Nitzan, J. Chem. Phys. 78, 5324 (1983).
9. L. Allen and J. H. Eberly, Optical Resonance and Two-Level Atoms (Wiley, New York, 1975), pp. 28-78.
10. B. R. Mollow, Phys. Rev. 188, 1969 (1969).
11. X. Y. Huang, J. Lin and T. F. George, J. Chem Phys. 80, 893 (1984).
12. X. Y. Huang and T. F. George, J. Phys. Chem.88, 4801 (1984).
13. X. Y. Huang, K. C. Liu and T. F. George, in Laser-Controlled Chemical Processing of Surfaces, ed. by A. W. Johnson, D. J. Ehrlich and H. R. Schlossberg (Elsevier, New York), Mat. Res. Soc. Symp. Proc. 29, 381 (1984).
14. X. Y. Huang, T. F. George and J. Lin, in Coherence and Quantum Optics V, ed. by L. Mandel and E. Wolf (Plenum, New York, 1984) pp. 685-693.
15. J. Lin, X. Y. Huang and T. F. George, Solid State Commun. 47, 63 (1983).
16. J. Gersten and A. Nitzan, J. Chem. Phys. 73, 3023 (1980).
17. A. C. Pineda and D. Ronis, J. Chem. Phys. 83, 5330 (1985).

18. P. M. Morse and H. Feshbach, Methods of Theoretical Physics (McGraw-Hill, New York, 1953), p. 1284.

19. G. C. Schatz, in Surface-Enhanced Raman Scattering, ed. by R. K. Chang and T. E. Furtak (Plenum, New York, 1983), p. 35.

Figure Captions

1. Geometry of the surface protusion. The semi-major axis is a and the semi-minor axis is b. The prolate spheroidal coordinates are defined by a scale factor, f, given by $f = (a^2 - b^2)^{1/2}$.

2. Rough surface induced phase-decay constant γ_s as a function of the semi-minor axis b of the surface protusion, where the semi-major axis is fixed at 100 A. γ_s is in the unit of Einstein's spontaneous decay constant A.

3. Time evolution of the population inversion in the weak-field or large-detuning limit with $(\gamma_L, \Omega, \Delta) = (0.3, 0.05, 5)$ in the unit of Einstein's spontaneous decay constant A for b = 34 A [Fig. 3(a)] and b = 38 A [Fig. 3(b)], with a fixed at 100 A. The horizontal axis corresponds to time in the unit A^{-1}. The quantity $[\omega(t) + 1]/\Omega^2$ is shown along the vertical axis. The curves numbered 1, 2, 3 and 4 correspond to the reduced atom-bump distance $\bar{d} = 20$, 25, 30 and 35, respectively ($\bar{d} = 2\pi d/\lambda$, where λ is the laser wavelength).

4. Resonance fluorescence power spectrum of scattered light with $(\gamma_L, \Omega, \Delta) = (0.3, 0.05, 5)$ in the unit A for b = 40 A [Fig. 4(a)] and b = 38 A [Fig. 4(b)]. Curves 1, 2 and 3 correspond to the reduced atom-bump distances $\bar{d} = 20$, 25 and 30, respectively. X denotes $(\omega - \omega_L)/(\omega_{21} - \omega_L)$ on the horizontal axis. The units along the vertical axis are arbitrary.

5. Strong-field surface-modified resonance fluorescence spectrum, where just the incoherent component of Rayleigh scattering is included, with $(\Delta, \Omega, b) = (1, 10, 38)$ for Fig. 5(a) and $(\Delta, \Omega, b) = (10, 10, 38)$ for Fig. 5(b), Δ and Ω are in the unit of A and b in the unit A. Curves 1, 2 and 3 correspond to the reduced atom-bump distances $\bar{d} = 20$, 25 and 30, respectively. X denotes $(\omega - \omega_L)/\Omega'$ on the horizontal axis. The units along the vertical axis are arbitrary.

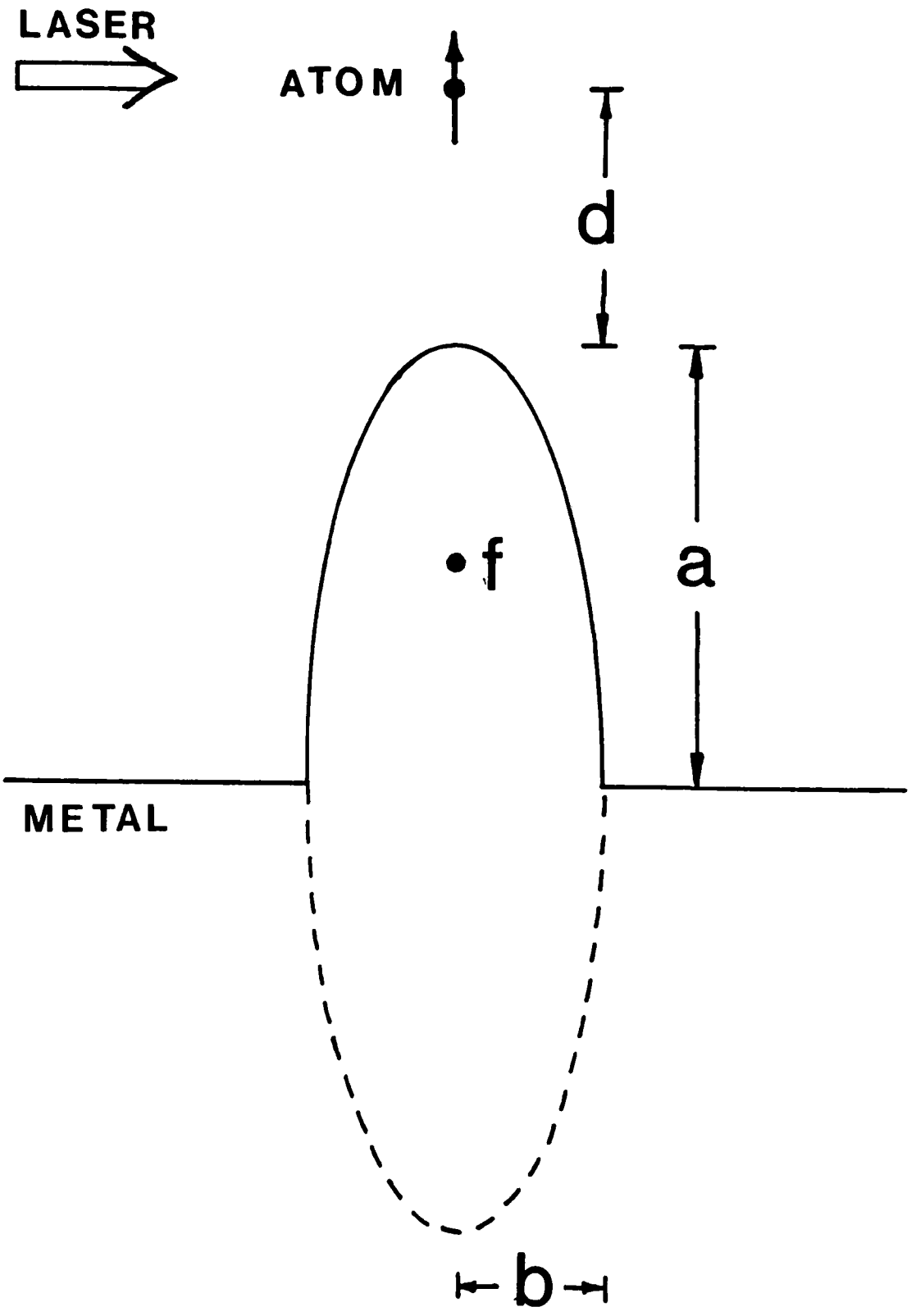
LASER
ATOM
d
a
f
METAL
b

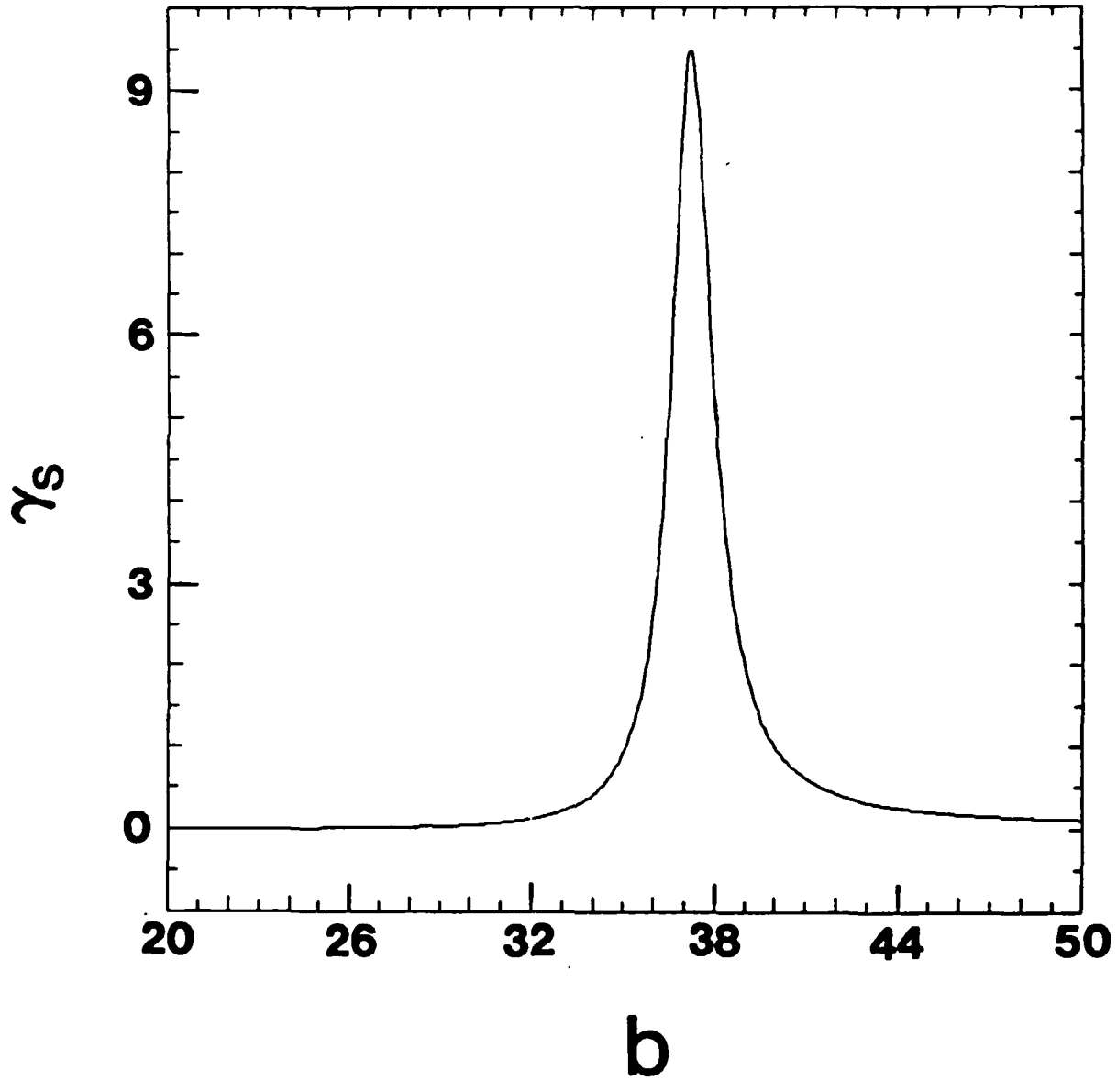

$\gamma_s - b$

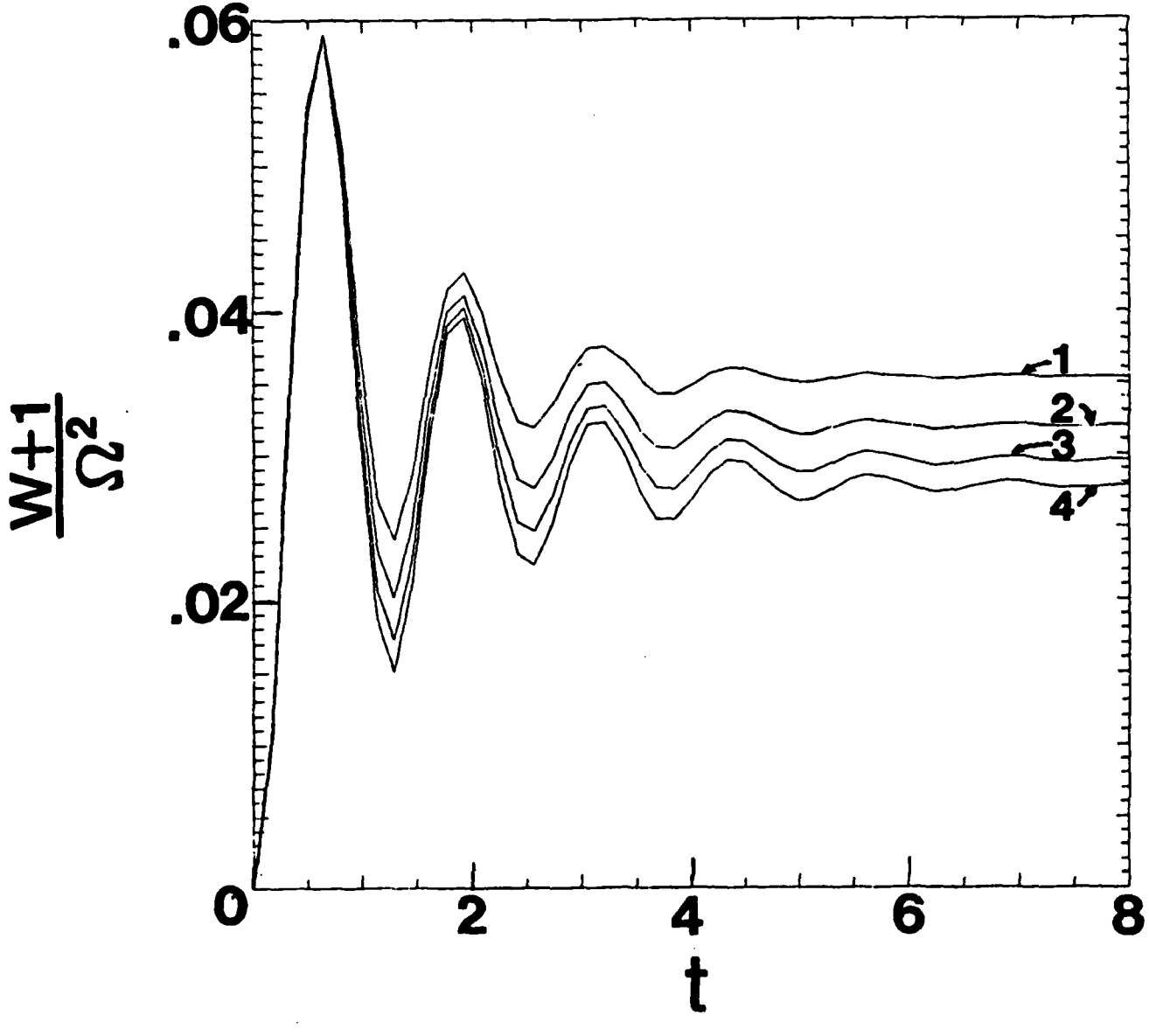
.06
.04
.02
0
2
4
6
8
t
W+1/Ω²
1
2
3
4

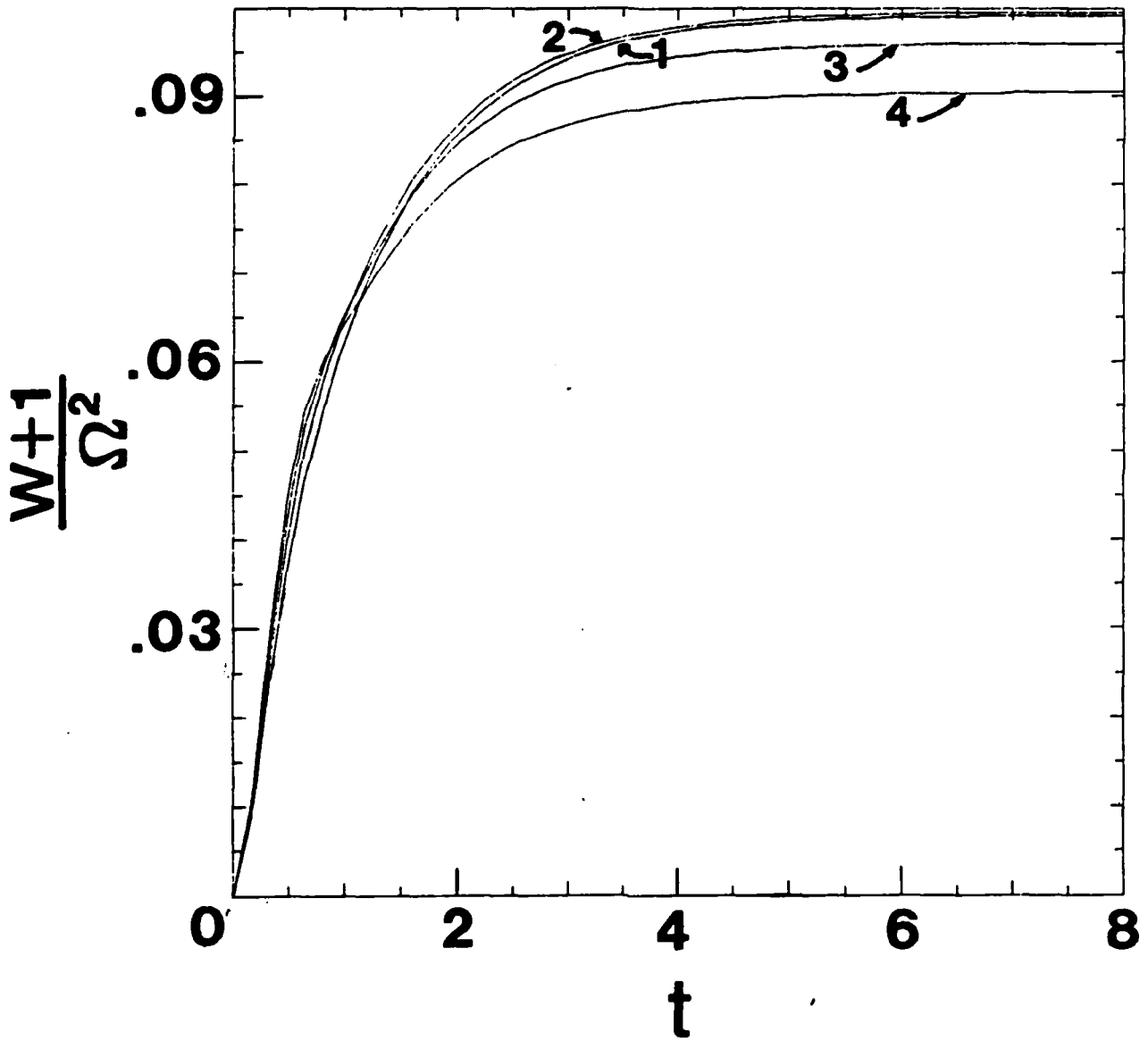

Fig. 3 – (b)

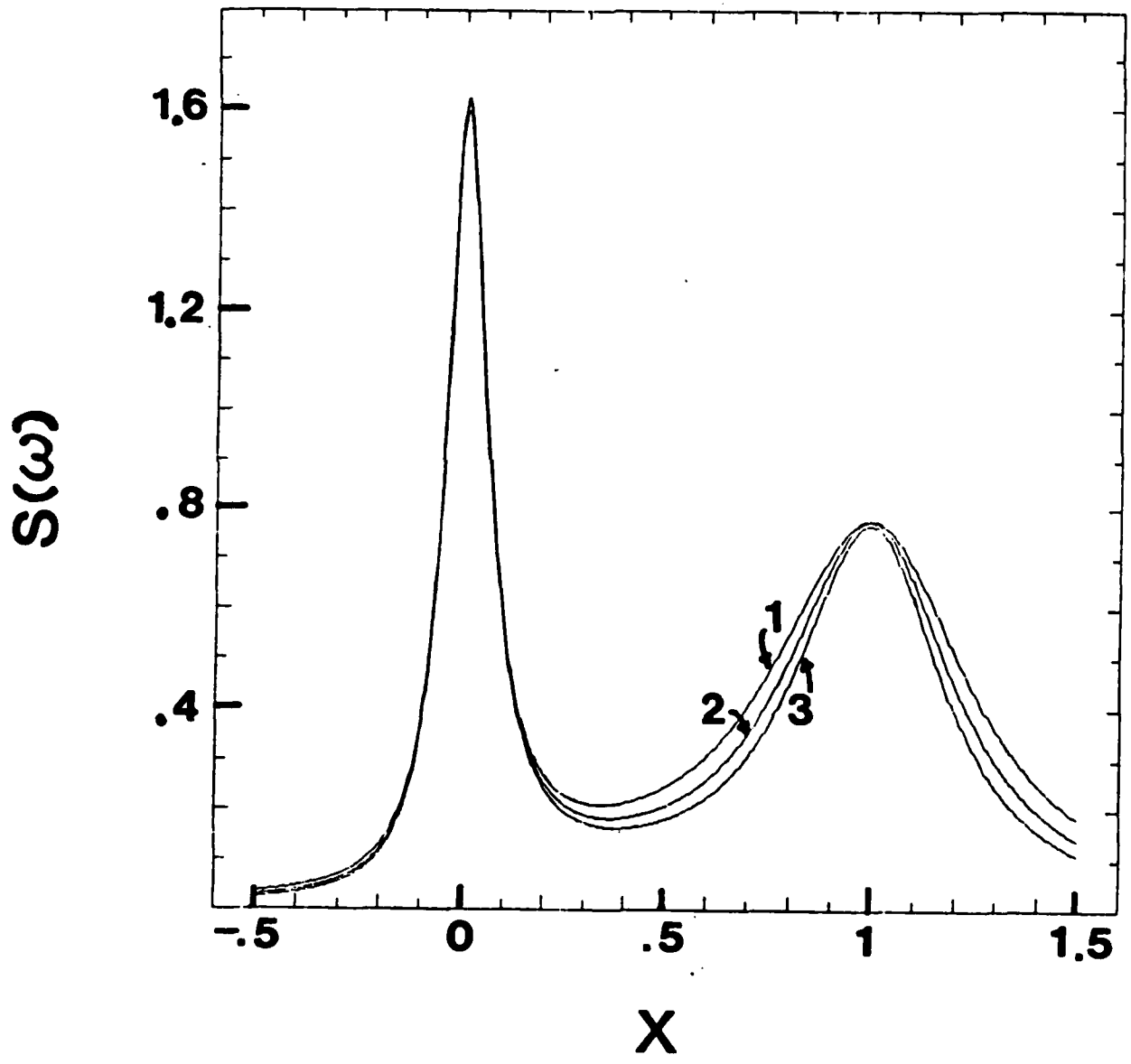
S(ω)
1.6
1.2
.8
.4
-.5
0
.5
1
1.5
X
1
2
3

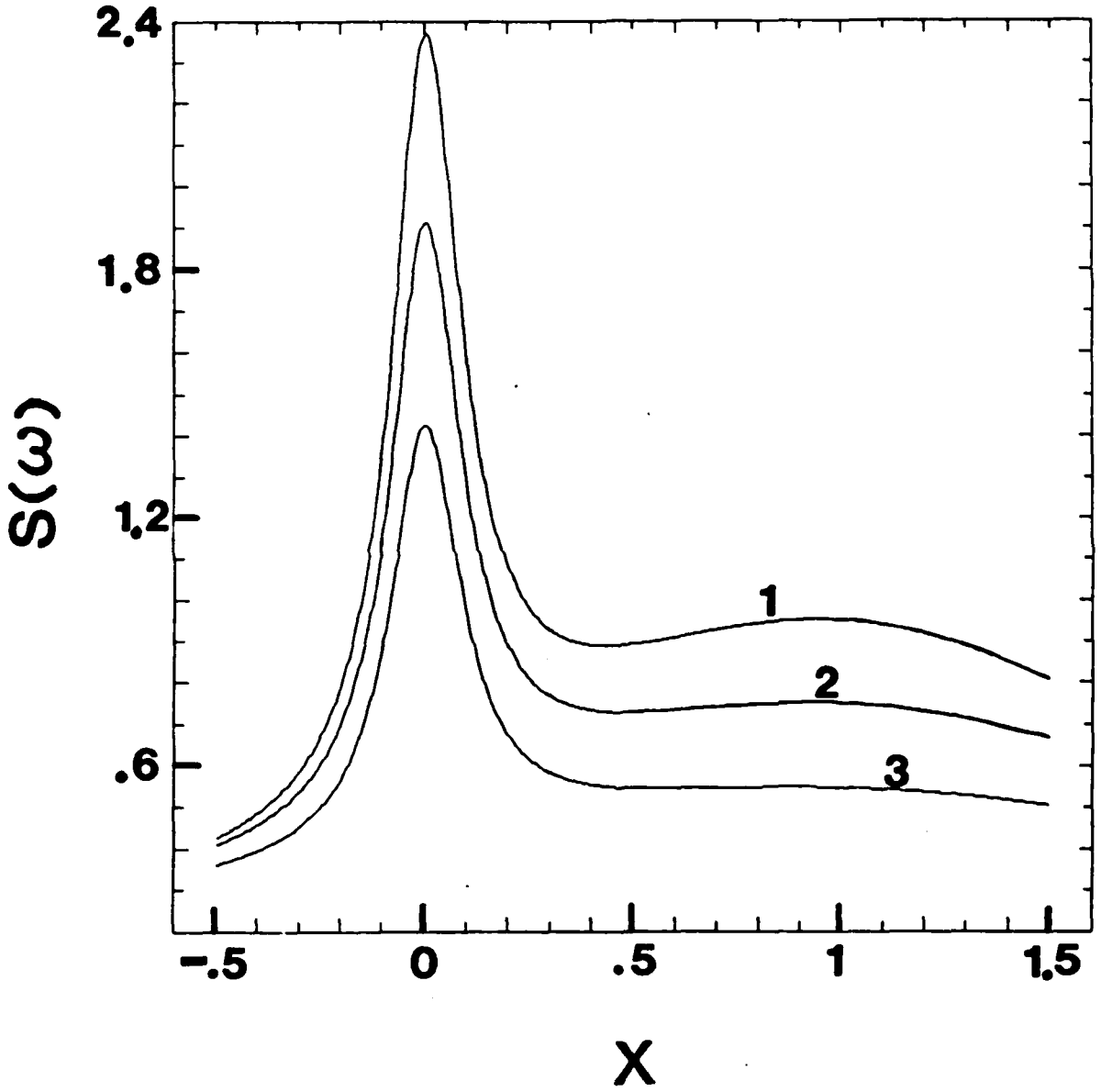

Fig 4(b)

Fig. 5.5 (a)

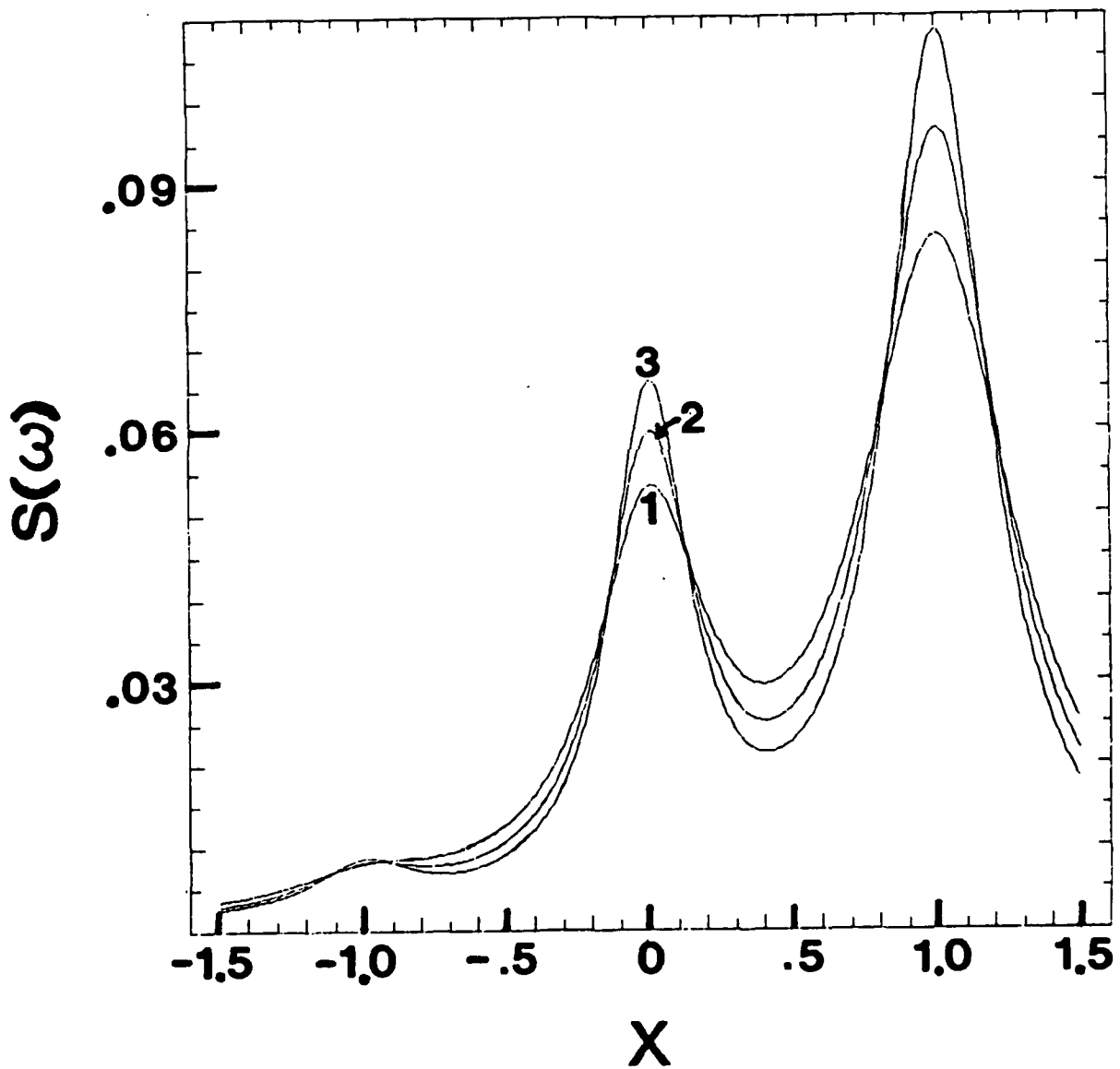
S(ω)
.09
.06
.03
3
2
1
-1.5
-1.0
-.5
0
.5
1.0
1.5
X

T. George ONR Technical Report Mailing List - 10/19/84

Office of Naval Research
Attn: Code 413
800 N. Quincy Street
Arlington, Virginia 22217

Dr. Bernard Douda
Naval Weapons Support Center
Code 5042
Crane, Indiana 47522

Defense Technical Information Center
Building 5, Cameron Station
Alexandria, Virginia 22314

Commander, Naval Air Systems
Command
Attn: Code 310C (H. Rosenwasser)
Washington, D.C. 20360

Dr. William Tolles
Superintendent
Chemistry Division, Code 6100
Naval Research Laboratory
Washington, D.C. 20375

Naval Civil Engineering Laboratory
Attn: Dr. R. W. Drisko
Port Hueneme, California 93401

Dr. David L. Nelson
Chemistry Division
Office of Naval Research
800 North Quincy Street
Arlington, Virginia 22217

DTNSRDC
Attn: Dr. G. Bosmajian
Applied Chemistry Division
Annapolis, Maryland 21401

Dr. J. Murday
Naval Research Laboratory
Surface Chemistry Division (6170)
455 Overlook Avenue, S.W.
Washington, D.C. 20375

Dr. David Young
Code 334
NORDA
NSTL, Mississippi 39529

T. George ONR Technical Report Mailing List - 10/19/84

Naval Weapons Center
Attn: Dr. Ron Atkins
Chemistry Division
China Lake, California 93555

Dr. G. A. Somorjai
Department of Chemistry
University of California
Berkeley, California 94720

Scientific Advisor
Commandant of the Marine Corps
Code RD-1
Washington, D.C. 20380

Dr. J. B. Hudson
Materials Division
Rensselaer Polytechnic Institute
Troy, New York 12181

U.S. Army Research Office
Attn: CRD-AA-IP
P.O. Box 12211
Research Triangle Park, NC 27709

Dr. Theodore E. Madey
Surface Chemistry Section
Department of Commerce
National Bureau of Standards
Washington, D.C. 20234

Mr. John Boyle
Maerials Branch
Naval Ship Engineering Center
Philadelphia, Pennsylvania 19112

Dr. J. E. Demuth
IBM Corporation
Thomas J. Watson Research Center
P.O. Box 218
Yorktown Heights, New York 10598

Naval Ocean Systems Center
Attn: Dr. S. Yamamoto
Marine Sciences Division
San Diego, California 91232

Dr. M. G. Lagally
Department of Metallurgical
and Mining Engineering
University of Wisconsin
Madison, Wisconsin 53706

T. George ONR Technical Report Mailing List - 10/19/84

Dr. R. P. Van Duyne
Department of Chemistry
Northwestern University
Evanston, Illinois 60201

Dr. W. T. Peria
Electrical Engineering Department
University of Minnesota
Minneapolis, Minnesota 55455

Dr. J. M. White
Department of Chemistry
University of Texas
Austin, Texas 78712

Dr. Keith H. Johnson
Department of Metallurgy
and Materials Science
Massachusetts Institute of Technology
Cambridge, Massachusetts 02139

Dr. D. E. Harrison
Department of Physics
Naval Postgraduate School
Monterey, California 93940

Dr. S. Sibener
Department of Chemistry
James Franck Institute
5640 Ellis Avenue
Chicago, Illinois 60637

Dr. W. Kohn
Department of Physics
University of California, San Diego
La Jolla, California 92037

Dr. Arnold Green
Quantum Surface Dynamics Branch
Code 3817
Naval Weapons Center
China Lake, California 93555

Dr. R. L. Park
Director
Center of Materials Research
University of Maryland
College Park, Maryland 20742

Dr. A. Wold
Department of Chemistry
Brown University
Providence, Rhode Island 02912

T. George ONR Technical Report Mailing List - 10/19/84

Dr. S. L. Bernasek
Department of Chemistry
Princeton University
Princeton, New Jersey 08544

Dr. R. Stanley Williams
Department of Chemistry
University of California
Los Angeles, California 90024

Dr. P. Lund
Department of Chemistry
Howard University
Washington, D.C. 20059

Dr. R. P. Messmer
Materials Characterization Lab
General Electric Company
Schenectady, New York 12301

Dr. F. Carter
Code 6132
Naval Research Laboratroy
Washington, D.C. 20375

Dr. Robert Gomer
Department of Chemistry
James Franck Institute
5640 Ellis Avenue
Chicago, Illinois 60637

Dr. Richard Colton
Code 6112
Naval Research Laboratory
Washington, D.C. 20375

Dr. Ronald Lee
R301
Naval Surface Weapons Center
White Oak
Silver Spring, Maryland 20910

Dr. Dan Pierce
Optical Physics Division
National Bureau of Standards
Washington, D.C. 20234

Dr. Paul Schoen
Code 5570
Naval Research Laboratory
Washington, D.C. 20375

T. George ONR Technical Report Mailing List - 10/19/84

Dr. R. G. Wallis
Department of Physics
University of California
Irvine, California 92717

Dr. J. T. Keiser
Department of Chemistry
University of Richmond
Richmond, Virginia 23173

Dr. D. Ramaker
Department of Chemistry
George Washington University
Washington, D.C. 20052

Dr. Roald Hoffman
Department of Chemistry
Cornell University
Ithaca, New York 14853

Dr. J. C. Hemminger
Department of Chemistry
Universit of California
Irvine, California 92717

Dr. R. W. Plummer
Department of Physics
University of Pennsylvania
Philadelphia, Pennsylvania 19104

Dr. G. Rubloff
IBM
Thomas J. Watson Research Center
P.O. Box 218
Yorktown Heights, New York 10598

Dr. E. Yeager
Department of Chemistry
Case Western Reserve University
Cleveland, Ohio 41106

Dr. Horia Metiu
Department of Chemistry
University of California
Santa Barbara, California 93106

Dr. N. Winograd
Department of Chemistry
Pennsylvania State University
University Park, Pennsylvania 16802

T. George ONR Technical Report Mailing List - 10/19/84

Dr. John T. Yates
Department of Chemistry
University of Pittsburgh
Rittsburgh, Pennsylvnia 15260

Dr. Adam Heller
Bell Laboratories
Murray Hill, New Jersey 07974

Dr. Richard Greene
Code 5230
Naval Research Laboratory
Washington, D.C. 20375

Dr. Martin Fleischmann
Department of Chemistry
Southampton University
Southampton SO9 5NH
Hampshire, England

Dr. L. Kesmodel
Department of Physics
Indiana University
Bloomington, Indiana 47403

Dr. John W. Wilkins
Laboratory of Atomic and
Solid State Physics
Cornell University
Ithaca, New York 14853

Dr. K. C. Janda
California Institute of Technology
Division of Chemistry and
Chemical Engineering
Pasadena, California 91125

Dr. Richard Smardzewski
Code 6130
Naval Research Laboratory
Washington, D. C. 20375

Dr. E. A. Irene
Department of Chemistry
University of North Carolina
Chapel Hill, North Carolina 27514

Dr. H. Tachikawa
Department of Chemistry
Jackson State University
Jackson, Mississippi 39217

T. George ONR Technical Report Mailing List - 10/19/84

Dr. A. Steckl
Department of Electrical and
Systems Engineering
Rensselaer Polytechnic Institute
Troy, New York 12181

Dr. J. E. Jensen
Hughes Research Laboratory
3011 Malibu Canyon Road
Malibu, California 90265

Dr. G. H. Morrison
Department of Chemistry
Cornell University
Ithaca, New York 14853

Dr. J. H. Weaver
Department of Chemical Engineering
and Materials Science
University of Minnesota
Minneapolis, Minnesota 55455

Dr. P. Hansma
Department of Physics
University of California
Santa Barbara, California 93106

Dr. W. Knauer
Hughes Research Laboratory
3011 Malibu Canyon Road
Malilbu, California 90265

Dr. J. Baldeschwieler
Division of Chemistry
California Institute of Technology
Pasadena, California 91125

Dr. C. B. Harris
Department of Chemistry
University of California
Berkeley, California 94720

Dr. W. Goddard
Division of Chemistry
California Institute of Technology
Pasadena, Califlornia 91125

Dr. A. Reisman
Microelectronics Center
of North Carolina
Research Triangle Park
North Carolina 04469

T. George ONR Technical Report Mailing List - 10/19/84

Dr. M. Grunze
Laboratory for Surface Science
and Technology
University of Maine
Orono, Maine 04469

Dr. F. Kutzler
Department of Chemistry
Box 5055
Tennessee Technological University
Cookesville, Tennessee 38501

Dr. J. Butler
Naval Research Laboratory
Code 6115
Washington DC 20375

Dr. D. DiLella
Chemistry Department
George Washington University
Washington DC 20052

Dr. L. Interante
Chemistry Department
Renssealer Polytechnic Institute
Troy, New York 12181

Dr. R. Reeves
Chemistry Department
Renssaeler Polytechnic Institute
Troy NY 12181

Dr. Irvin Heard
Chemistry and Physics Department
Lincoln University
Lincoln University, Pennsylvania 19352

Dr. David young
Code 334
NORDA
NSTL, Mississippi 39529

Dr. K. J. Klaubunde
Department of Chemistry
Kansas State University
Manhattan, Kansas 66506

END

FILMED

2-86

DTIC